Interaction Notes
Note 255

UNCLASSIFIED
SECURITY CLASSIFICATION OF THIS PAGE *(When Data Entered)*

REPORT DOCUMENTATION PAGE

READ INSTRUCTIONS BEFORE COMPLETING FORM

1. REPORT NUMBER: AFWL-TR-74-338	2. GOVT ACCESSION NO.
3. RECIPIENT'S CATALOG NUMBER	
4. TITLE *(and Subtitle)*: SELF-CONSISTENCY AND RADIATION ENHANCED GROUND CONDUCTIVITY IN THE SURFACE BURST CODE SCX	5. TYPE OF REPORT & PERIOD COVERED: Final Report
	6. PERFORMING ORG. REPORT NUMBER: SAI-74-505-AQ
7. AUTHOR(s): B. H. Fishbine, S. J. Dalich & J. N. Wood	8. CONTRACT OR GRANT NUMBER(s): F29601-74-C-0006
9. PERFORMING ORGANIZATION NAME AND ADDRESS: Science Applications Corp. 1200 Prospect Street, P.O. Box 2351 LaJolla, CA 92037	10. PROGRAM ELEMENT, PROJECT, TASK AREA & WORK UNIT NUMBERS: 62707H , WDNE 0707 Subtask: R99QAXEA094 Work Unit: 41
11. CONTROLLING OFFICE NAME AND ADDRESS: Director Defense Nuclear Agency Washington, DC 20305	12. REPORT DATE: November 1975 13. NUMBER OF PAGES: 54
14. MONITORING AGENCY NAME & ADDRESS *(if different from Controlling Office)*: Air Force Weapons Laboratory Air Force Systems Command Kirtland AFB, NM 87117	15. SECURITY CLASS. *(of this report)*: Unclassified 15a. DECLASSIFICATION/DOWNGRADING SCHEDULE

16. DISTRIBUTION STATEMENT *(of this Report)*

Approved for public release; distribution unlimited.

17. DISTRIBUTION STATEMENT *(of the abstract entered in Block 20, if different from Report)*

18. SUPPLEMENTARY NOTES

This research was sponsored by the Defense Nuclear Agency under Subtask R99QAXEA094, Work Unit 41, Work Unit Title Low Altitude Predictions.

19. KEY WORDS *(Continue on reverse side if necessary and identify by block number)*

Electromagnetic Pulse (EMP)
High Altitude EMP
EMP Code Development
EMP Prediction Techniques

20. ABSTRACT *(Continue on reverse side if necessary and identify by block number)*

A description of the numerical techniques used to include the self-consistent effect in the two-dimensional ground burst EMP code, SCX, is given. The effect of this phenomenon on the fields predicted by SCX is discussed and illustrated. The effect is most notable for observer positions less than 2,000 meters from the burst point where a sign change occurs in the transverse E field.

DD FORM 1 JAN 73 1473 EDITION OF 1 NOV 65 IS OBSOLETE

UNCLASSIFIED
SECURITY CLASSIFICATION OF THIS PAGE *(When Data Entered)*

Also presented are discussion and results concerning the inclusion of a radiation enhanced ground conductivity model in SCX. Results of calculations with this model indicate that for a zero height of burst situation, field effects are minimal.

TABLE OF CONTENTS

LIST OF FIGURES

LIST OF FIGURES (Continued)

SECTION I
INTRODUCTION

SCX is a two dimensional ground burst EMP (electromagnetic pulse) computer code. The general numerical methods used in the code are documented[1] elsewhere and will not be discussed here. Briefly, the code obtains the solution to Maxwell's equations in the source region of a surface nuclear burst. Because the solution is obtained in the source region, several nonlinearities are inherent to the problem. First, the conductivity of the medium depends strongly on the total electric field. The effect has always been modeled in the code. Second, the source terms are themselves influenced by the fields. This effect is generally referred to as "self-consistency", and until recently was not included in the SCX code. This paper reviews the methods used to model self-consistency in SCX, and presents comparative results of calculations before and after the effect was included in SCX.

An exact representation of self-consistency requires the solution to the equations of motion for the Compton electrons. Clearly, for an EMP computer code with two space dimensions plus time, this is impractical. The amount of storage required is not available, and the running time would render the code economically useless. Fortunately, methods have been devised which allow for the inclusion of the self-consistent effect in an approximate fashion[2]. These methods require a minimal amount of storage and cause only slight increases in running time.

The sources of the EMP are the Compton recoil electrons created through the device radiation interactions with the atmosphere. In SCX these sources are described as current densities in the radial and transverse directions. The current densities were obtained from Monte Carlo transport calculation results which were then curve fit for use in the code. The transport results, being completely independent of the EMP calculation, do not contain any effects due to interactions with

electromagnetic fields. To include the self-consistent effect, some modification must be made to the source terms within the SCX code. This leads to several necessary approximations, the impact of which will be discussed below.

SECTION II
A DESCRIPTION OF THE SELF-CONSISTENCY MODEL

The self-consistency model used is derived from EMP Theoretical Note 77, Volume 2-4, by H. J. Longley.[2] The note describes a way of modifying a purely radial, analytic current source to obtain self-consistent radial and transverse currents. The method is based on electron turning in the presence of electromagnetic fields.

To determine the amount of turning, a group of electrons is followed in various time constant electromagnetic environments. These electrons are recoils created by Compton scattered, monoenergetic gamma rays and are chosen to represent a physically realistic distribution of Compton recoil angles and energies. The equations of motion for the electrons are differenced and solved numerically. The computation proceeds in time until an electron's kinetic energy is within 1% of its rest mass energy. In STP air, 1 MeV electron has a range of .49 g/cm^2. An electron with a kinetic energy equal to 10% of its rest mass energy, has a range of .0049 g/cm^2. So a 1 MeV electron slowed to 1% of its rest mass energy is easily within .1% of its final range. At this point, the electron's final radial and transverse positions are recorded. An average is taken of the final positions for the group of electrons and these averages are used to obtain self-consistent currents. The validity of this method depends on the lifetimes of the electrons and the time steps used in the SCX calculation. This matter will be discussed later.

To obtain the self-consistent radial current, the original radial, analytic current is multiplied by DX/R_{mf} where DX is the average electron final radial position and R_{mf} is the mean forward range of the electron in the absence of fields. The self-consistent transverse current is obtained by multiplying the original radial current by DY/R_{mf}, where DY is the average electron final transverse position. In the earth's magnetic field, the Larmor radius of a 1 MeV electron is about 100 times

its range. Since typical EMP fields produce much greater effects, such as reversing the transverse current obtained from Monte Carlo transport calculations, the geomagnetic field will be neglected.

Two items are important in this method. The first is the initial kinetic energy, E_e, of an electron to be tracked. This energy depends on the initial gamma energy, $E_{\gamma o}$, and the scattering angle and is obtained directly from the Klein-Nishina equation. The second item of importance is the calculation of R_{mf}. R_{mf} is the mean forward range obtained by

$$R_{mf} = \frac{1}{\sigma_c} \int_{\theta_e = 0}^{\pi/2} R \cos \theta_e \sigma_e d\Omega_e \qquad (1)$$

where

$$\sigma_c = \int_{\theta_e = 0}^{\pi/2} \sigma_e d\Omega_e \qquad (2)$$

and σ_e is the angular differential cross-section obtained from the Klein-Nishina formula, $d\Omega_e$ is the solid angle associated with the scattering angle θ_e of the recoil electron, θ_e is the angle between the initial direction of propagation of the gamma and the direction of the electron's recoil. R is the range obtained from a fit to experimental mean range versus energy data. The energy used to obtain R is E_e which is a function of $E_{\gamma o}$ and θ_e.

Our method of obtaining self-consistent currents is different in several respects from the method described in EMP Theoretical Note 77. Where Longley's method used only an analytic, radial current source; the current sources used in SCX have both radial and transverse components. The general method described in Note 77 is designed for use with an analytic current source. The source terms in SCX are, however, not analytic, having been obtained through curve fits to the results of gamma and neutron Monte Carlo transport calculations. The source terms serve as inputs to SCX, and are expressed

as total currents in the radial and transverse directions. In order to adapt the general method to our purposes, tables similar to Longley's were generated. However, our tables are for electrons recoiling in the same direction as the initial gamma propagation direction and are not averages of electrons recoiling at different θ_e. This was done because the transport calculations which provide the current sources for SCX already include angular scatter effects and the electron energy spectrum is already folded in.

In applying DX/R and DY/R factors to the SCX transport derived currents, first a total initial current is calculated from the initial transport derived radial and transverse currents. This total current is then treated in the same manner that the analytic radial current source is treated in Longley's method. To accomplish this, the angle between the positive radial axis and the total initial current is used to transform the radial and transverse electric fields to a new primed coordinate system where the total initial current is parallel to the primed positive radial axis (i.e., a transformation to a coordinate system in which the transverse current is zero). The DX/R and DY/R factors are applied to the total initial current and the resulting primed self-consistent radial and transverse currents are transformed back to the original coordinate system to obtain the final self-consistent currents.

In addition to following single electrons rather than probabilistically representative groups, our method differs from Longley's in two respects. First, rather than using the initial electron kinetic energy calculated directly from the Klein-Nishina equation, a mean initial electron energy is used. This energy is calculated by

$$\bar{E}_e = \frac{1}{\sigma_c} \int_{\theta_e=0}^{\pi/2} E_e \sigma_e \, d\Omega_e$$

Where E_e is a function of θ_e and initial gamma energy, $E_{\gamma o}$, and is calculated from the Klein-Nishina equation.

Secondly, the range we use is different from R_{mf}, the mean forward range used by Longley. We use a range R_c, which is the electron range calculated by the electron tracking subroutine with all fields set to zero. This range differs from the range obtained by using $\bar{E}_e$ and the R in Eqn. (1) only because of roundoff error.

In Longley's scheme, tables of DX and DY were generated for various field values and gamma energies. These tables were then fit by analytic functions and the functions used to introduce self-consistency into the LEMP code. In our case, tables of DX/R_c and DY/R_c are generated and used directly by SCX, along with some interpolation coding, to obtain self-consistency. The interpolation scheme is simple-minded and chosen to supply smooth sources to SCX.

The interpolation is basically as follows. The three field values calculated by SCX are the radial electric field (E_r); the transverse electric field (E_θ) and the phi magnetic field (B_ϕ). These fields can be thought of as the three coordinates of a field space. For the DX/R_c tables each entry in the table represents a point in the field space. Similarly for DY/R_c. For a given set of field values calculated by SCX, the interpolation coding determines what eight points, the vertices of a rectangular solid, corresponding to given DX/R_c or DY/R_c surround the point P whose coordinates are given by the three field values. This rectangular solid can be broken up into eight sub-solids by passing three planes through the fields value point. The planes are parallel to the six faces of the original solid and generate one sub-solid for each vertex of the original solid. The interpolation scheme weights the DX/R_c or DY/R_c value at a particular vertex by a volume obtained by subtracting the volume of the sub-solid of that vertex from the volume of the original solid. This weighting is done for all eight points, summed and divided by the total volume of the original solid. The scheme is smooth and has the advantage

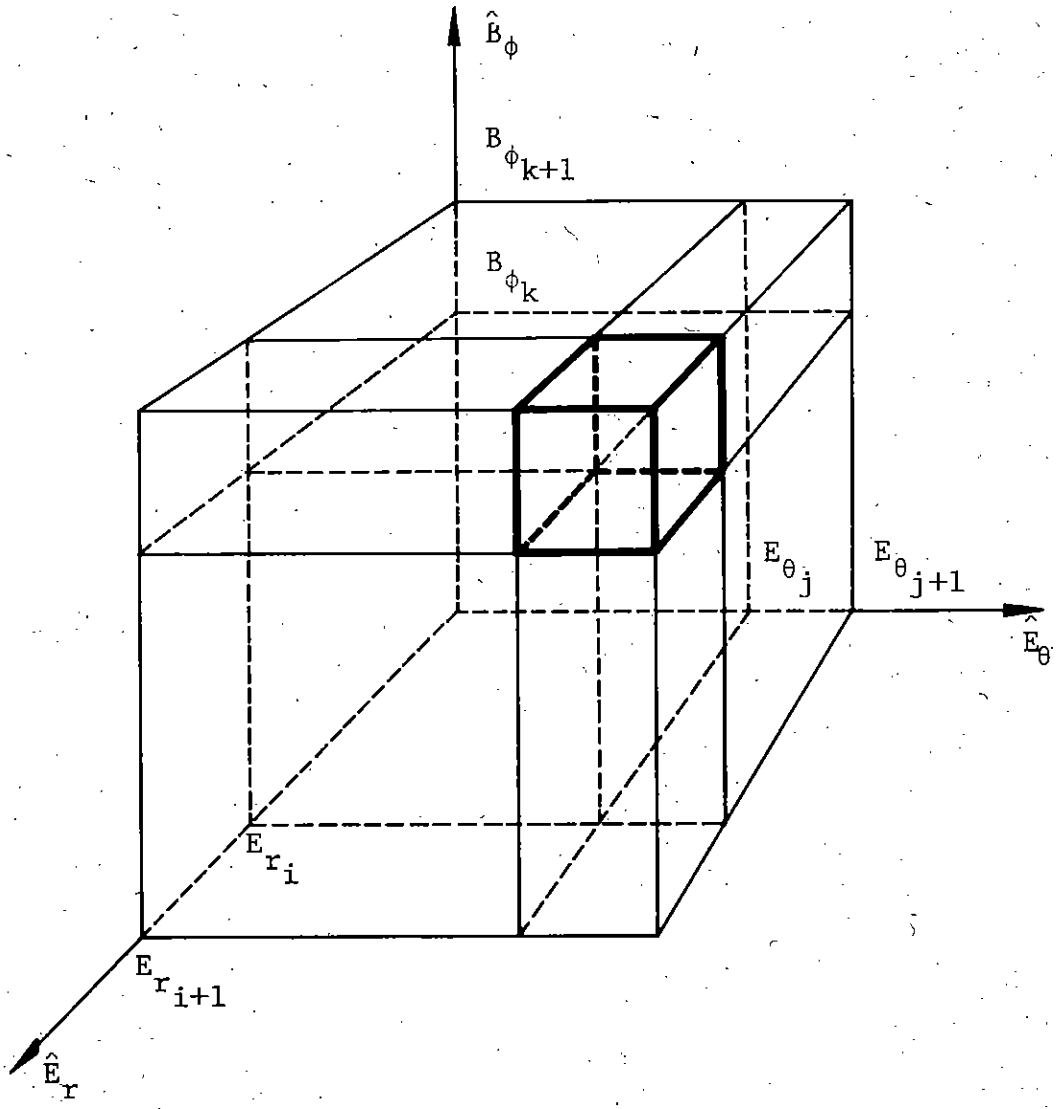

Fig. 1. The field space used in the interpolation scheme.

that if the fields values fall exactly on a point in the tables, the precise values of DX/R_c and DY/R_c from the tables are obtained.

The equation of motion used in the electron tracker subroutine is:

$$\vec{p} = -|e| \left\{ \vec{E} + \vec{v} \times \vec{B} \right\} - A \frac{\vec{p}}{|\vec{p}|}$$

where $\vec{p}$ is the electron's momentum, e the electron's charge, $\vec{v}$ the electron's velocity, $\vec{E}$ the electrical intensity of the environment, $\vec{B}$ the magnetic intensity, and A is a slowing term like $\frac{dE}{ds}$ which includes energy losses due to ionization, multiple scattering and radiation. If $\vec{E}$ and/or $\vec{B}$ are large enough their contributions will overcome the energy loss term A and the electrons will never come to rest. These are termed run-away electrons. The self-consistency model used here includes a range of field values which generate DX/R_c and DY/R_c tables that exclude run-away electrons. Therefore, the interpolation coding holds field values to the limits used in generating the tables.

In estimating the effect of self-consistency on the conductivity we have to consider the effects of the electric fields on an electron's kinetic energy, since the kinetic energy determines the amount of ionization. If an electron has an initial velocity in a given direction an electric field parallel to the velocity vector will increase or decrease the electron's kinetic energy depending on the sign of the field.

Generally, the direction of the radial electric field is positive, away from the burst source point. Similarly for the Compton recoil electrons. Therefore, the radial electric field tends to reduce the recoil electron energy and thereby reduce the ionization due to electrons. Initially the theta electron velocity in the transformed system is zero so that the theta electric field will increase the electron's theta momentum

regardless of the field's sign. These approximate arguments lead to the following correction factor, f_q, to the ionization rate.

$$f_q = \frac{\bar{E}_e + W}{\bar{E}_e}$$

where

$$W = |e| \left\{ |E_\theta DY| - E_r DX \right\}$$

and $|e|$ is the absolute value of the electron's charge. W is an estimate of the work done by the fields on the electron and therefore changes the energy available for ionization.

The applicability of this self-consistent scheme is questionable when the time steps used by fields code differencing are comparable or less than the lifetimes of the electrons. In real time, for gammas of 1.5 MeV, electron lifetimes are on the order of 10^{-8} second. In retarded time, due to turning, this time may be much larger since there is a component of the electron velocity which is parallel to the gamma wave front.

In a typical SCX run, the time steps during the prompt gamma peak are 10^{-9} second. After the peak, time steps are 10^{-8} second and larger. By examining electron trajectories for typical SCX environments it is apparent that the electrons frequently turn back and complete loops. But it is still likely that the final position of an electron is in the same general direction from the electron's original position as the position of an electron at the end of a time step shorter than the electron's lifetime. Since the electron is slowing down, we expect that the electric fields, at least, will have more effect on the electron's position near the end of its life than at the beginning where it has large kinetic energy. In the present SCX calculations, the self-consistent effect is probably exaggerated during the prompt gamma peak.

An approximate correction in such situations might be to scale the turning by a factor $t_s/t_{e\ell}$, where t_s is the time step and $t_{e\ell}$ is the electron lifetime. A better factor would be

$$f_t = (t_s/t_{e\ell})^2$$

which more heavily weights time steps close to $t_{e\ell}$. The f_t factor is plausible because the non-relativistic equation for a displacement s due to a constant force on a mass m is

$$s = \frac{F}{2m} t^2 .$$

The f_t factor would scale the angle that the position vector of the electron's final position makes with the initial gamma propagation direction. To accomplish this, take the original DX/R_c and DY/R_c. Compute

$$\alpha = \left\{ [DY/R_c] \; / \; [DX/R_c] \right\} = \tan \delta$$

$$m = \left\{ [DX/R_c]^2 + [DY/R_c]^2 \right\}^{\frac{1}{2}}$$

$$\beta = \arctan \left\{ \alpha \cdot f_t \right\}$$

$$[DX/R_c]' = m \cos (\beta)$$

$$[DY/R_c]' = m \sin (\beta)$$

and use $[DX/R_c]'$ and $[DY/R_c]'$ as before.

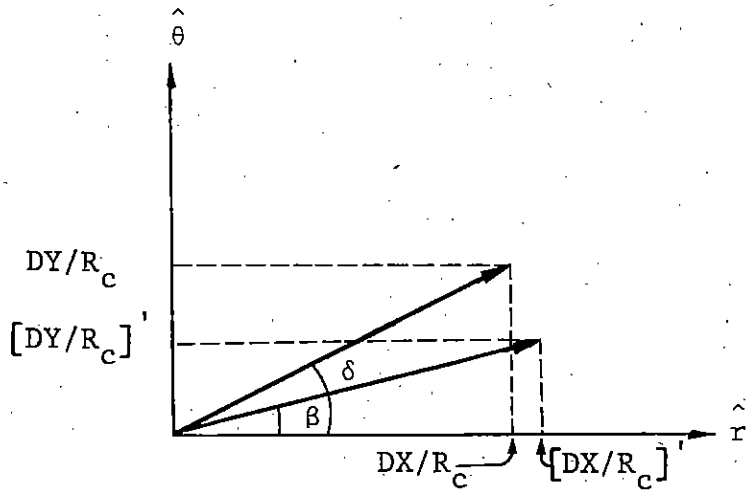

Fig. 2. Scaling Self-Consistent Currents by the Time-Step Factor.

SECTION III
THE EFFECT OF SELF-CONSISTENCY ON THE CURRENTS

To interpret the plots overlaying self-consistent and non-self-consistent time histories of SCX runs, it is useful to first describe the individual effects of the fields on a single electron.

For an electric field $\vec{E}$, the force on a charge q is $\vec{F} = \vec{E}\,q$. An electron in a positive E_r field experiences a force in the $-\hat{r}$ direction which contributes to a positive radial conventional current. Since the Compton recoil electrons are streaming radially outward, constituting a negative conventional current, the isolated effect of a positive E_r field is to reduce the magnitude of the negative radial current $-J_r$. The same type of argument indicates the effect of E_θ on the theta current.

SCX calculates a B_ϕ which is negative. Since $|J_r|$ is usually greater than $|J_\theta|$, we first consider the effect of a magnetic field on a purely radial current.

An electron with a velocity $\vec{v}$ in the $+\hat{r}$ direction will experience a magnetic force $\vec{F} = q(\vec{v} \times \vec{b})$. For B_ϕ negative $\vec{F}$ will be in the $-\hat{\theta}$ direction and so contribute to a positive theta conventional current.

Occasionally, J_r and J_θ are the same order of magnitude. In the extreme case where the conventional current is purely in the $-\theta$ direction, the magnetic field will contribute to a negative radial conventional current.

In determining whether it is an electric field or the magnetic field which dominates the electron turning, it is useful to be able to make rough comparisons between the effects of the electric and magnetic fields.

For an electron of initial energy $\bar{E}_e$, initial speed v_o, and absolute charge e, we define F_m to be the maximum magnetic force on the electron and F_s to be the maximum slowing force on the

electron. Since these two forces are monotonically increasing functions of the electron velocity, (except for F_s when the electron energy is below 0.5 MeV) the maxima occur at the electron's maximum speed, i.e., v_o. For an incident gamma of 1.5 MeV, E_e is .75 MeV and v_o is 2.75×10^8 m/sec. F_m and F_s can then be compared as follows:

$$F_m/e = B_\phi \cdot 2.75 \times 10^8$$

$$F_s/e = \frac{A(v)_o}{e} = 3.49 \times 10^5$$

The slowing term $A(v_o)$ is obtained from a fit to experimental data of electron energy as a function of electron mean range. This fit is differentiated with respect to range to obtain $\frac{dE}{ds}$.

With the use of F_m and F_s we can predict the combination of effects of the various fields on the currents.

The radial current overlays in Figs. 3 and 12 show that for ranges of 500m and 1000m the self-consistent model reduces the magnitude of the radial current until past a microsecond. This is especially noticeable at the time of the prompt gamma peak and also past 10 shakes where the reduction in J_r increases markedly with time until near a microsecond. The 2000m radial currents overlay exactly, which prompts us to consider the close-in ranges and the 2000m range separately. Evidently, at 2000m for this yield, the fields are reduced enough to show only small self-consistent effects, primarily in J_θ and E_θ.

As mentioned earlier, the effect of a positive E_r field is to reduce the magnitude of a negative J_r. For the two close-in ranges, E_r is positive throughout the calculation. Also, a negative B_ϕ will only increase the magnitude of negative J_r when J_θ is negative and $|J_\theta| \sim |J_r|$. In the self-consistent case, we see that $|J_r|/|J_\theta|$ is close to unity at 12 μsec. At this point, in Fig. 3, the self-consistent J_r is increased as expected. By comparing the

non-self-consistent J_θ and J_r, it is seen that separation between the self-consistent J_r and non-self-consistent J_r continues to increase.

The more pronounced $-J_r$ reduction at the time of the prompt gamma peak is due to the combined peaking of E_r and B_ϕ. After the prompt gamma pulse, whereas E_r is saturated and remains reasonably constant out to neutron arrival at around 10 microseconds, B_ϕ steadily increases in magnitude and thus increases the separation of the J_r overlays. It is interesting to note that at 500m the self-consistent B_ϕ starts leveling off at around 2 μsec and then starts to decrease at about 5 μsec. The separation in the J_r overlays follows this behavior until the non-self-consistent J_θ becomes larger than the non-self-consistent J_r. Similar behavior is shown at 1000m.

At 2000m there is no visible effect of the self-consistent model on the radial current. This is plausible on the basis of rough field comparisons. The maximum value of E_r at this range is 5×10^3. The maximum absolute value of B_ϕ is 3×10^{-4}. In this case, F_m/e is $\sim 8 \times 10^4$. Since F_s/e is $\sim 3.5 \times 10^5$, it seems reasonable that the self-consistent effect on J_r due to E_r will be negligible, and the effect due to B_ϕ will be small, particularly since at this range, $|J_r| >> |J_\theta|$ and nearly all the kinetic energy of the electron is in the radial direction.

The self-consistent theta currents for the two close-in ranges show three interesting features. First, while the non-self-consistent theta currents are always negative, the self-consistent theta currents are nearly always positive. Second, the self-consistent theta currents follow the prompt gamma pulse in a much more obvious fashion than the non-self-consistent theta currents. Third, after the prompt gamma pulse, the self-consistent theta currents dip and then exhibit a gentle bump, and finally change sign after 10 microseconds.

The self-consistent theta currents are nearly always positive because B_ϕ nearly always predominates over E_θ and the non-self-consistent J_r is nearly always greater than the non-self-consistent

J_θ. There is a very short span of time at very early times where E_θ predominates. If values of E_θ and F_m/e are compared at 3 shakes in the usual manner, the E_θ dominance can be shown. In this tiny region of E_θ dominance, the self-consistent theta currents are negative. This situation is shown in Figs. 5 and 14.

That the theta currents are almost entirely determined by B_ϕ is further demonstrated by the jagged time behavior of E_θ and consequent smearing of the prompt gamma pulse. In contrast, the theta currents are smooth and follow the gamma pulse quite well because close-in the shape of the gamma pulse is preserved in B_ϕ.

Finally, the dip and gentle bump behavior is exhibited in B_ϕ but, due to the obvious non-linear relationship of electron turning to the magnitude of B_ϕ, the similarity of shape between the self-consistent J_θ and B_ϕ is not compelling, especially as the waveforms approach 10 μsec where the non-self-consistent J_θ becomes comparable to or greater than the non-self-consistent J_r. Beyond 10 μsec J_θ crosses over due to the fact that the non-self-consistent J_θ becomes comparable to or greater than (at 500m) the non-self-consistent J_r. In this region the effect of B_ϕ is to increase $-J_r$, as explained above, and so E_θ dominates J_θ behavior. E_θ starts its dominance before 10 μsec. The effect is to reverse J_θ. At 12 μsec and 500m (Fig. 9) and 22 μsec and 1000m (Fig. 18) E_θ crosses over and becomes positive. This causes the self-consistent J_θ to hump over as it heads for another cross-over.

At 2000m, rough field comparison shows that E_θ should dictate J_θ behavior. First, a vestige of the gamma pulse is seen in J_θ. The shape of the gamma pulse is preserved in E_θ but not in B_ϕ. Second, J_θ is uniformly negative as is E_θ past the start of the gamma pulse. Later in time B_ϕ rises faster than E_θ and at its peak there is a corresponding dip in J_θ because, as shown earlier, a negative B_ϕ acting on a negative J_r contributes to a positive J_θ.

Now it remains to examine the effects of the self-consistent model on the fields and the conductivity.

SECTION IV
THE EFFECT OF SELF-CONSISTENCY ON THE FIELDS

A few words should be said regarding the occasional raggedness of some of the fields. By examining range plots of E_θ, it is clear that choosing the inner boundary condition $E_\theta = 0$ is inappropriate. Originally this condition was chosen with the assumption that the inner boundary is a perfect conductor. This assumption is certainly inconsistent with the use of non-zero theta currents at the inner boundary. Range plots of E_θ at early times show a drastic discontinuity between the inner boundary and the first point out in range. In fact, E_θ is increasing in an exponential fashion toward the inner boundary rather than decreasing to zero. After a few time steps, this discontinuity develops into oscillations of E_θ in range. In turn these oscillations affect J_θ which feeds back into E_θ. To minimize these oscillations, a range current smoother has been installed in SCX. This stopgap measure is helpful but not completely effective as can be seen in the time plots of E_θ near the prompt gamma pulse.

In addition, the calculation of the conductivity involves using a field dependent electron mobility which is clearly affected by the erratic behavior of E_θ. The conductivity's slightly ragged behavior is fed back into E_r and into B_ϕ. This problem should be cleared up, if not eliminated, by a more physically realistic choice of inner boundary condition for E_θ, possibly something as simple-minded as:

$$E_\theta = -J_\theta/\sigma$$

The three equations of importance in SCX are, in retarded time, at $\theta = 90^\circ$ (on the ground)

4

$$1) \qquad \frac{1}{\mu r}\frac{\partial B_\phi}{\partial \theta} = J_r + \sigma E_r + \varepsilon_o \frac{\partial E_r}{\partial \tau}$$

$$2) \qquad -\frac{1}{\mu r}\left[\frac{\partial}{\partial r}(rB_\phi) - \frac{1}{c}\frac{\partial}{\partial \tau}(rB_\phi)\right] = J_\theta + \sigma E_\theta + \varepsilon_o \frac{\partial E_\theta}{\partial \tau}$$

$$3) \qquad \frac{1}{r}\left[\frac{\partial}{\partial r}(rE_\theta) - \frac{1}{c}\frac{\partial}{\partial \tau}(rE_\theta) - \frac{\partial}{\partial \theta}E_r\right] = -\frac{\partial B_\phi}{\partial \tau}$$

The usual arguments used to predict the time behavior of E_r from 1) are as follows. With the magnetic term negligible, at very early times J_r, σ and E_r are very small and so σE_r is negligible relative to J_r. Hence, the E_r behavior is predicted to be: $E_r = -\frac{1}{\varepsilon}\int J_r d\tau$.

After a time, σE_r becomes comparable to $-J_r$. Physically, this is described as occurring when the Compton current is cancelled by the conduction current. When this condition occurs $\frac{\partial E_r}{\partial \tau}$ is negligible, assuming the effects of the airground asymmetry have not yet allowed B_ϕ to diffuse into the region of interest. If J and σ rise initially as $e^{\alpha t}$, E_r saturates, i.e., $\frac{\partial E_r}{\partial \tau}$ is small, for $\sigma > \alpha\varepsilon_o$, where ε_o is the free space permitivity. For an α of 2×10^8, saturation occurs where $\sigma > 1.77 \times 10^{-3}$ and the time of saturation can be determined by examining Figs. 6, 15 and 23. For 500 and 1000 meters, saturation occurs before the prompt gamma peak. At 2000 meters, saturation never occurs.

How accurately E_r follows $-J_r/\sigma$ is estimated by a "relaxation time" which amounts to ε_o/σ. If σ is large enough, the relaxation time is so short that E_r does in fact follow J_r/σ, most visibly at late times where J_r/σ changes. At far ranges or closer in at very late times, σ is so small that the relaxation time is too large to follow J_r/σ.

Furthermore, at the close-in ranges, 500 and 1000m, saturation occurs before the prompt gamma peak so that E_r also peaks, and at far ranges, 2000m, saturation occurs after the prompt gamma peak so that the peak is not preserved in E_r by following J_r/σ, but rather from $E_r = \frac{-1}{\varepsilon_o}\int J_r d\tau$. For E_r, this results in a peak more broad and delayed in time from the prompt gamma peak. In certain time domains, some of these arguments are equally applicable to E_θ.

At 500m and 1000m, saturation occurs before the prompt gamma peak. The plots of σ at these ranges show that the self-consistent model doesn't greatly change the conductivity. However, E_θ, through the field-dependent electron mobility, introduces some small jaggedness into σ.

Since $E_r = -J_r/\sigma$ until past neutron arrival where σ is greatly reduced, thus increasing the relaxation time, it is reasonable that the $1/\sigma$ dependence of E_r greatly exaggerates the jaggedness in σ. Since J_r is reduced by self-consistency, E_r is reduced as well.

An interesting portion of the E_r curve is at and past neutron arrival. The σ curves show a sharp discontinuity in slope at neutron arrival and a subsequent characteristic hump. E_r exhibits this same slope discontinuity and an inverted hump out to about 30 μsec.

Close in, before the prompt gamma peak, E_θ is driven by the $\frac{\partial}{\partial\tau}(rB_\phi)$ term. At 500m and 1000m, this can be readily seen. In both self-consistent and non-self-consistent plots of E_θ there is a very smooth, sharp negative pulse which peaks at about 5 shakes. If this pulse were due to $-J_\theta/\sigma$ the E_θ pulse caused by a self-consistent J_θ would be opposite in sign to the E_θ pulse generated by a non-self-consistent J_θ. Examination of the slope of the B_ϕ curve shows that the E_θ pulse is in fact driven by $\frac{\partial}{\partial\tau}(rB_\phi)$. Between 3 and 5 shakes, B_ϕ rises rapidly and smoothly to a peak. Since B_ϕ is negative, an increasing $\frac{\partial}{\partial\tau}(rB_\phi)$ should give a negative E_θ value. It is clear from the non-self-consistent plots of E_θ that the pulse ends and a

sign change occurs at the point where B_ϕ peaks and turns over. After B_ϕ peaks, the slope of B_ϕ doesn't do anything of great interest until neutron arrival. In the intervening interval, E_θ is driven by $-J_\theta/\sigma$ as can be accurately verified by comparing $-J_\theta/\sigma$ with actual values of E_θ.

An important difference shown in the overlay plots of E_θ at 500m and 1000m is that, whereas E_θ remains positive for a long time after the negative pulse for the non-self-consistent case, E_θ remains negative for the self-consistent case. Here E_θ is just following $-J_\theta/\sigma$.

At 2000m, an interesting feature is that while self-consistency reduces the magnitude of J_θ due to B_ϕ, the self-consistent E_θ is actually larger than the non-self-consistent E_θ at times greater than 10 shakes. Here E_θ is not driven by J_θ.

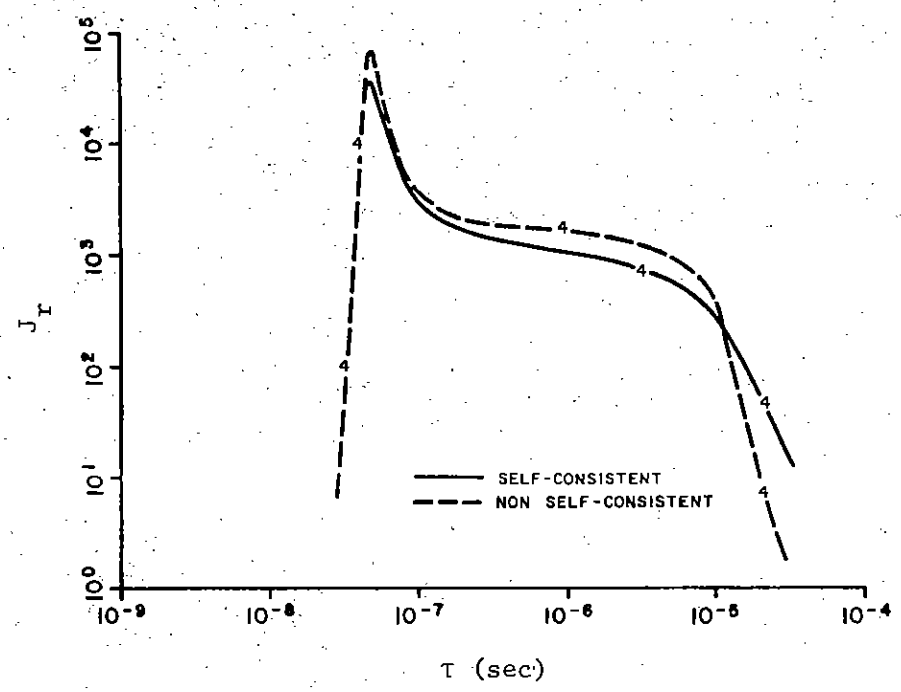

Fig. 3. Overlay of non-self-consistent and self-consistent radial currents at 500m, on the ground.

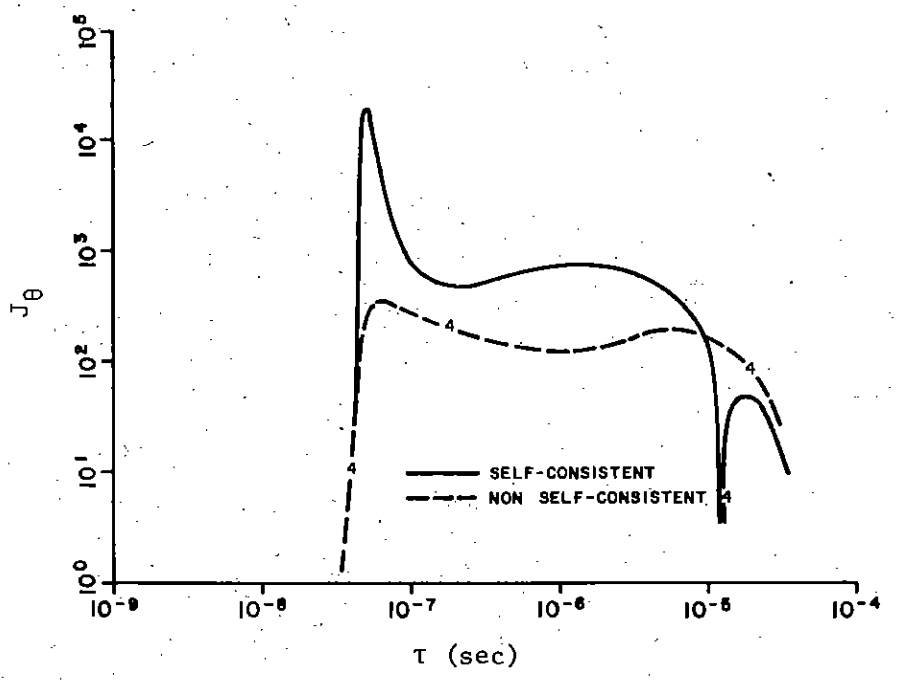

Fig. 4. Overlay, theta currents, 500m.

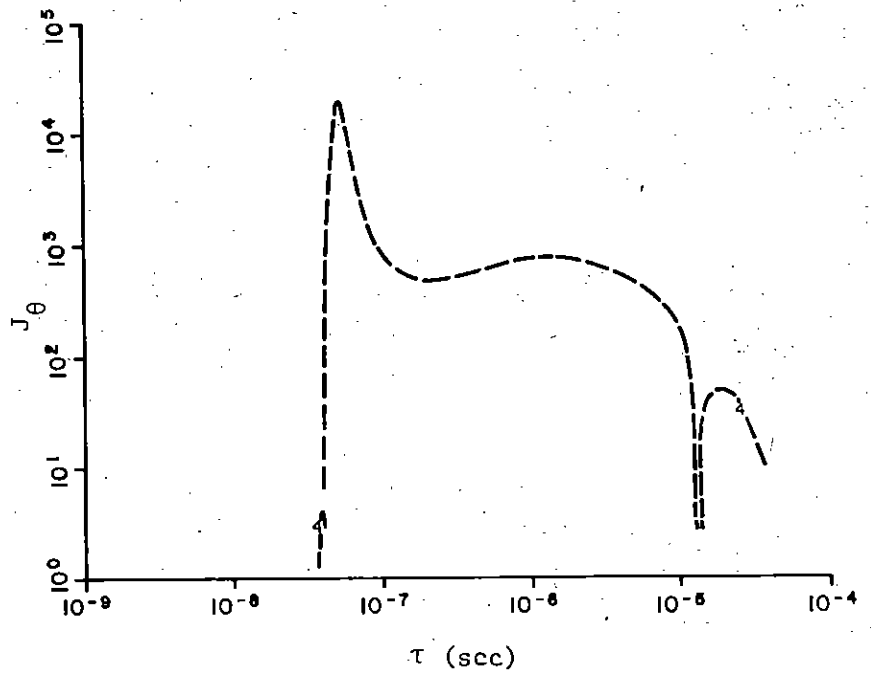

Fig. 5. Self-consistent theta current at 500m, on the ground.

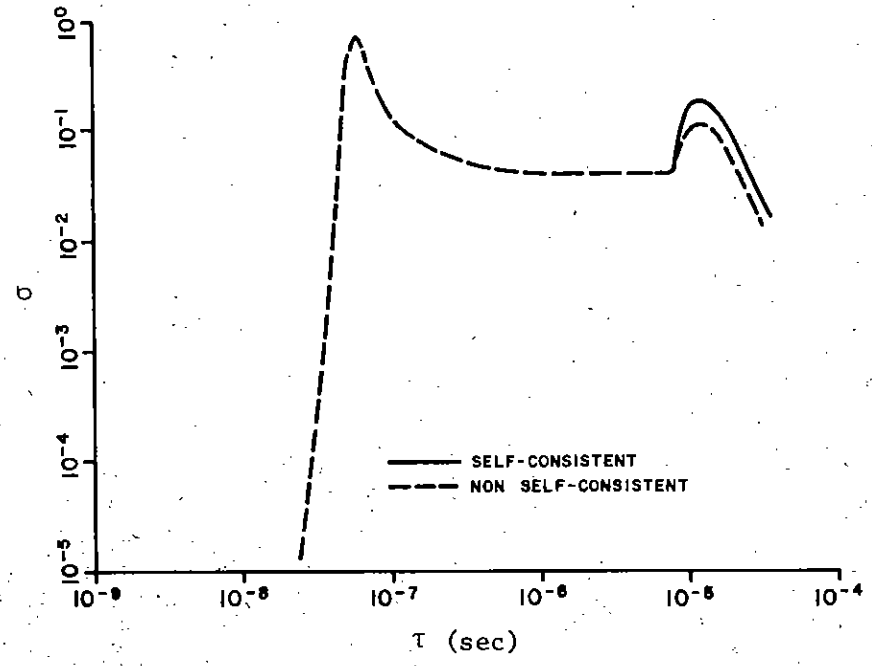

Fig. 6. Overlay, conductivities, 500m.

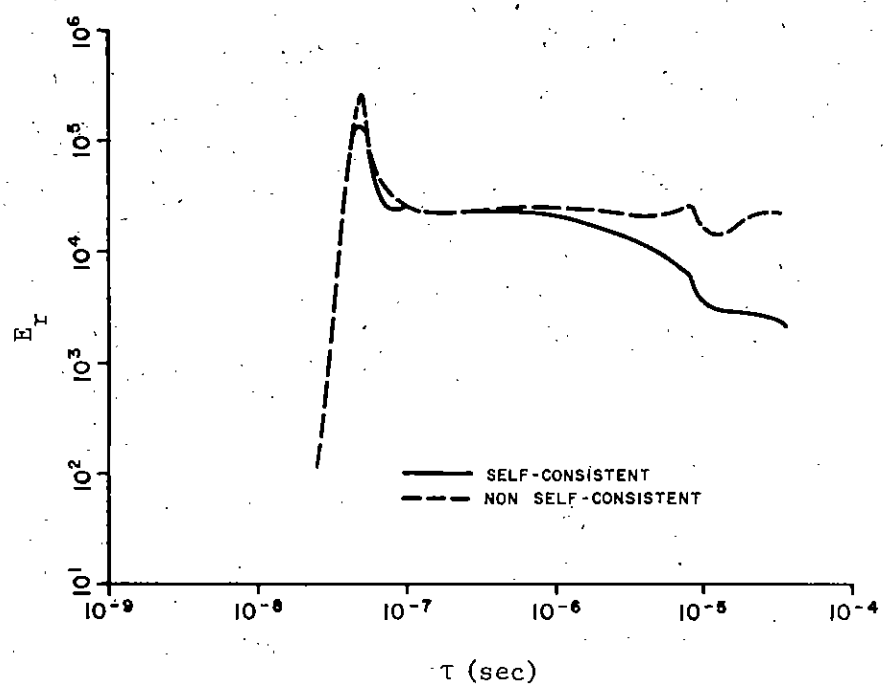

Fig. 7. Overlay, radial electric fields, 500m.

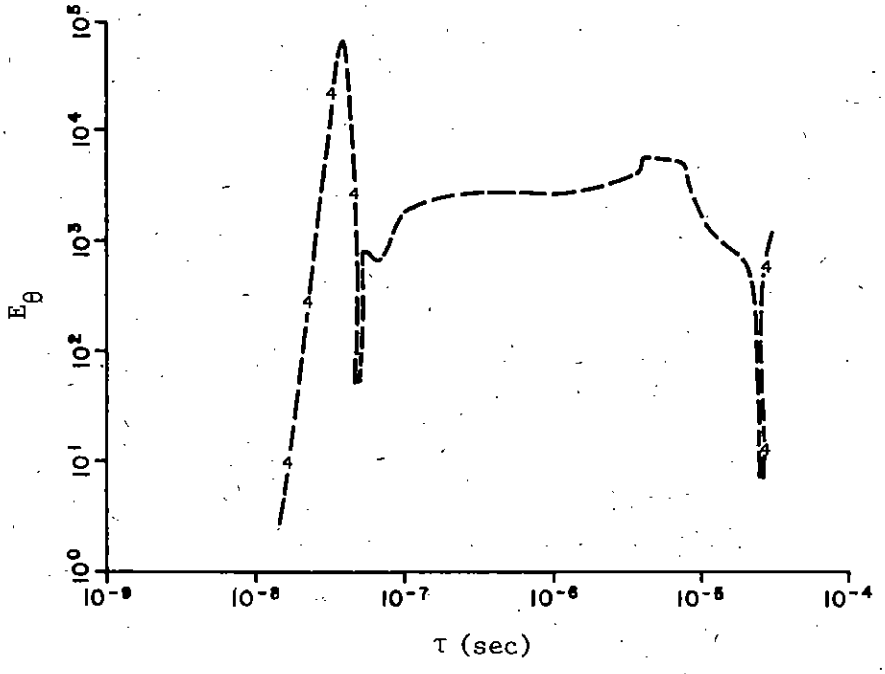

Fig. 8. Non-self-consistent theta electric field at 500m, on the ground.

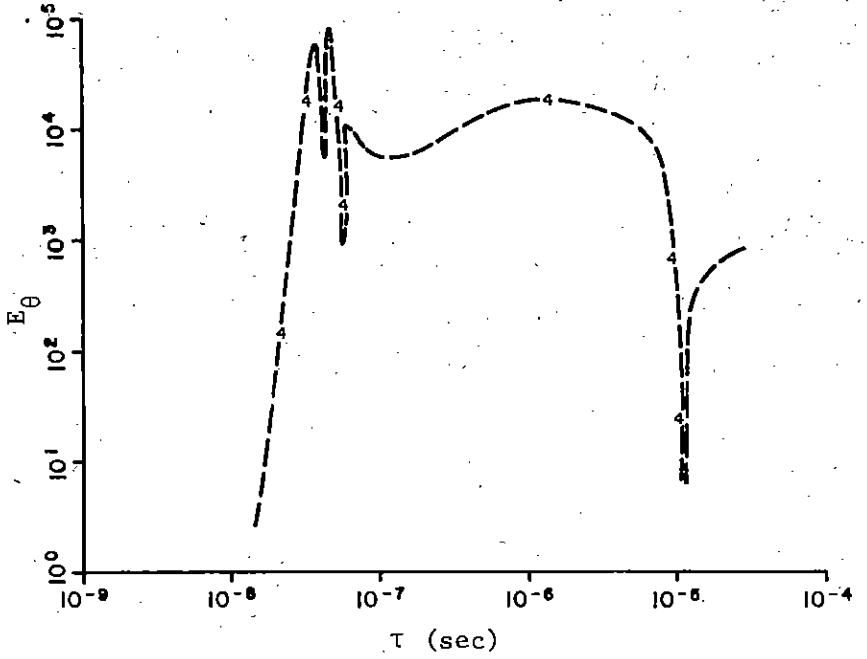

Fig. 9. Self-consistent theta electric field at 500m, on the ground.

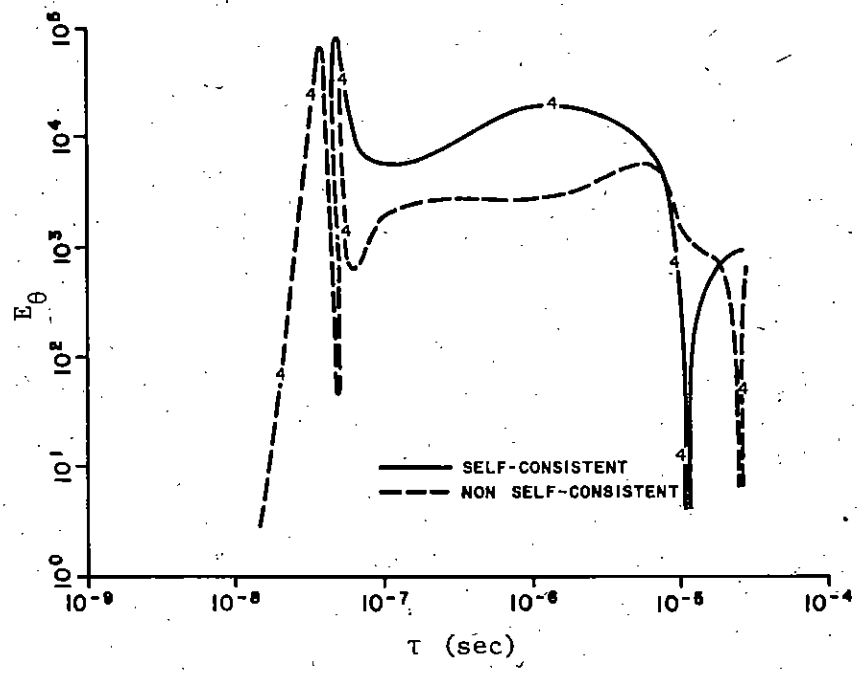

Fig. 10. Overlay, theta electric fields, 500m.

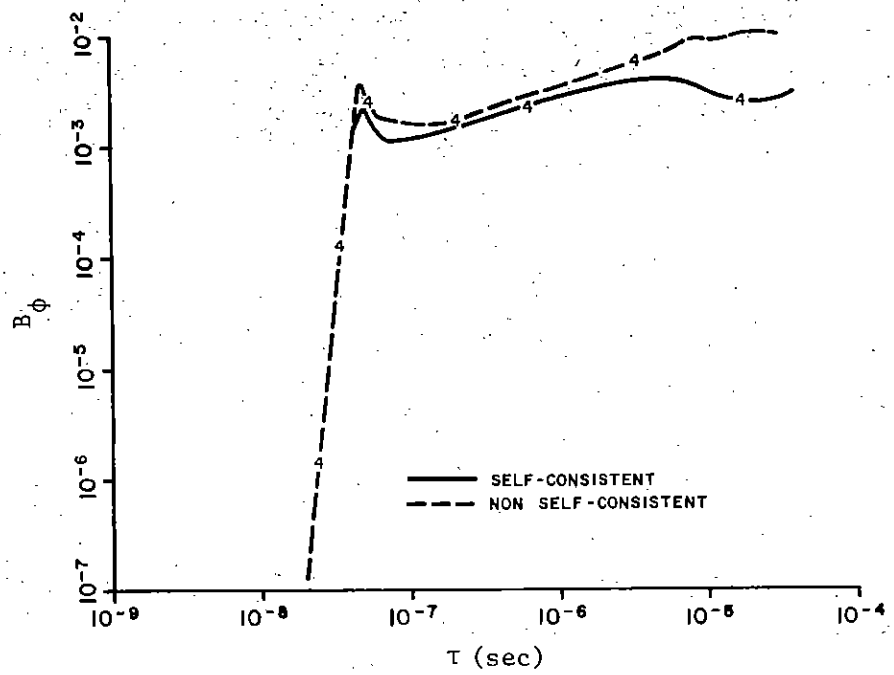

Fig. 11. Overlay, axial magnetic field, 500m.

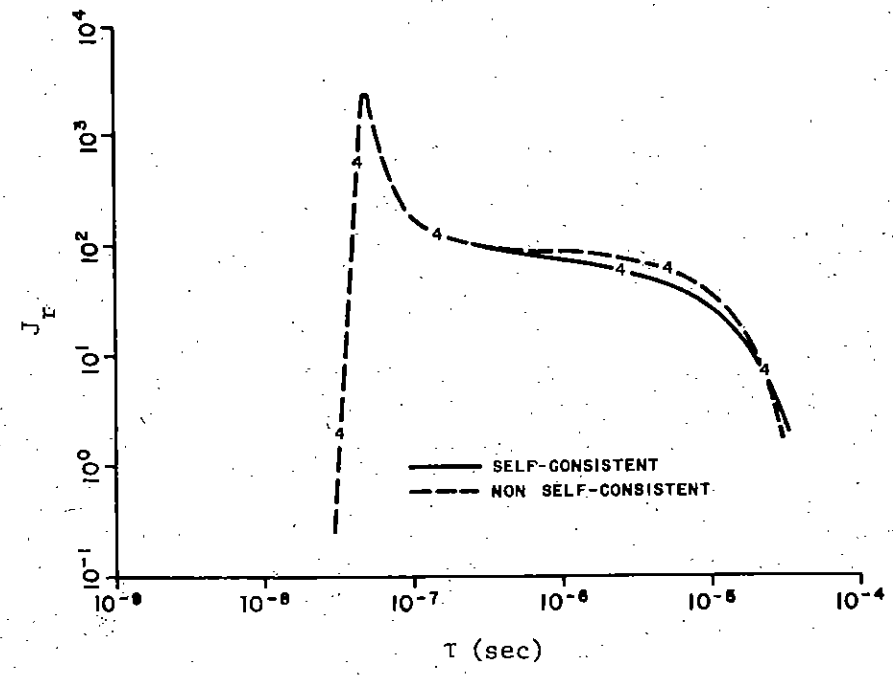

Fig. 12. Overlay, radial currents, 1000m.

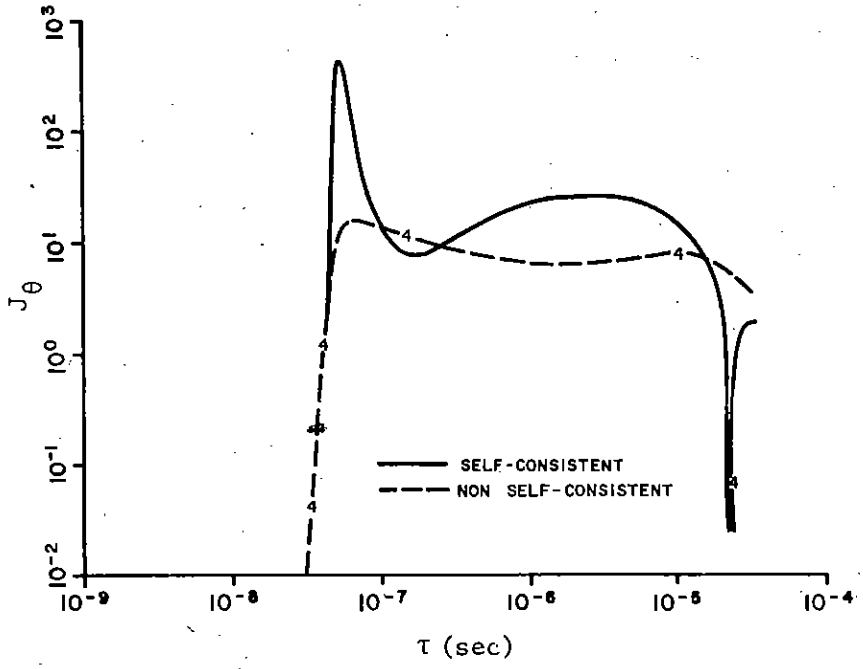

Fig. 13. Overlay, theta currents, 1000m.

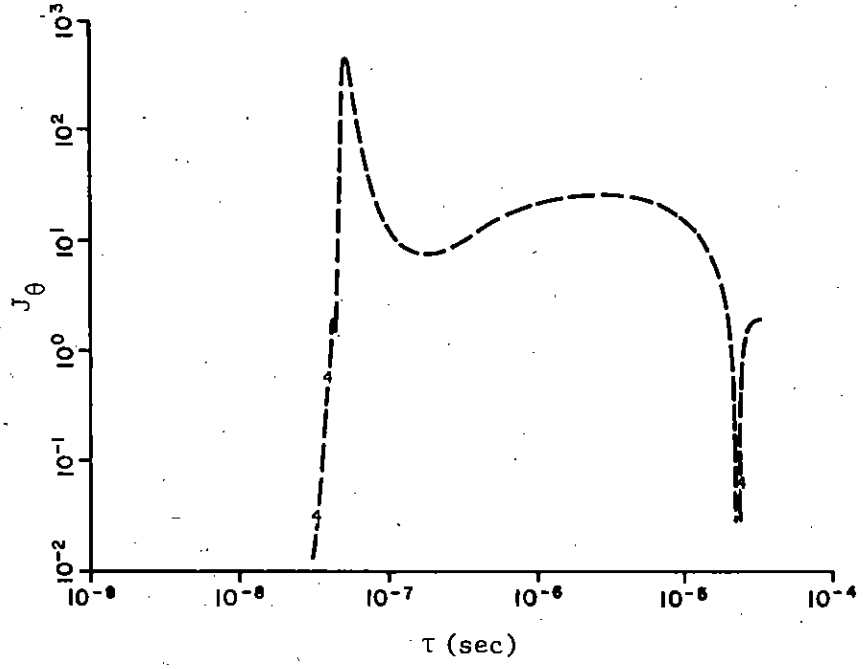

Fig. 14. Self-consistent theta current at 1000m, on the ground.

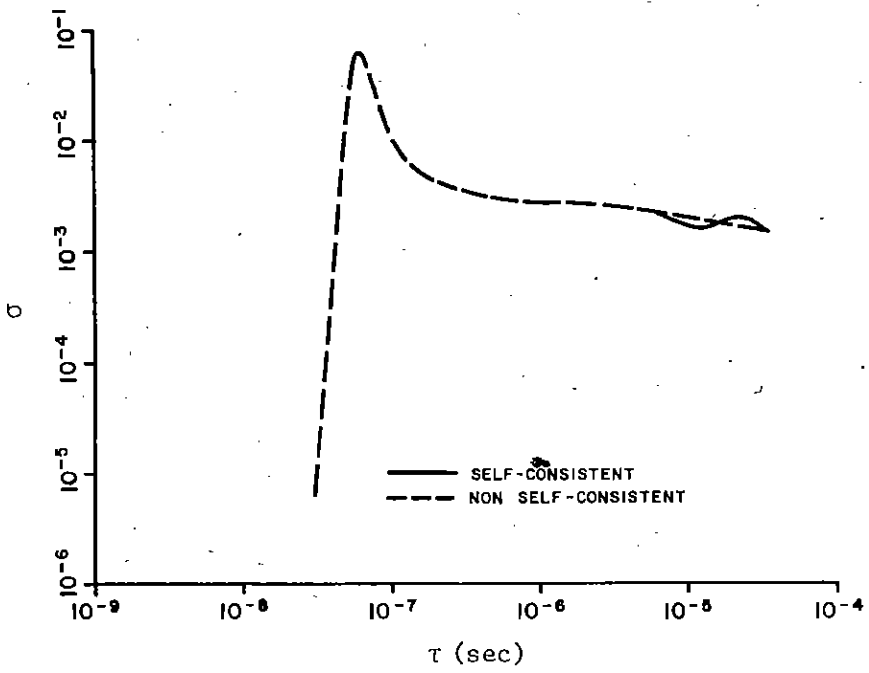

Fig. 15. Overlay, conductivities, 1000m.

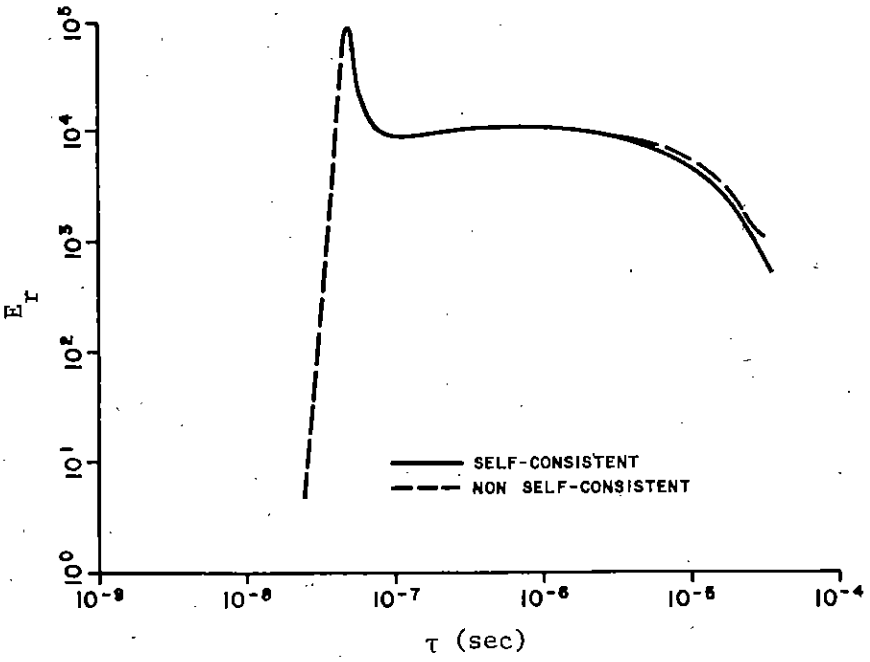

Fig. 16. Overlay, radial electric fields, 1000m.

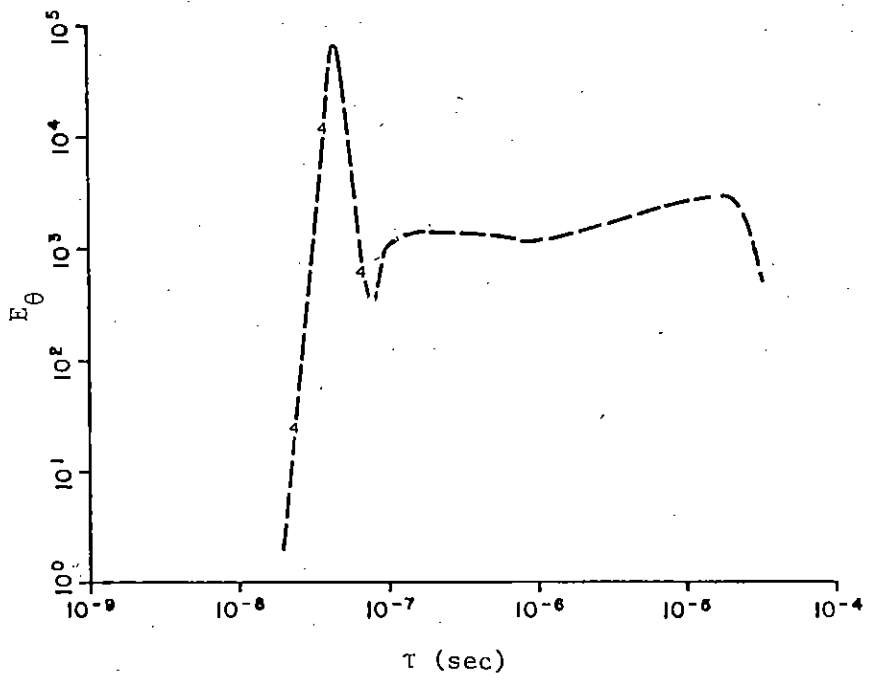

Fig. 17. Non-self-consistent theta electric field at 1000m, on the ground.

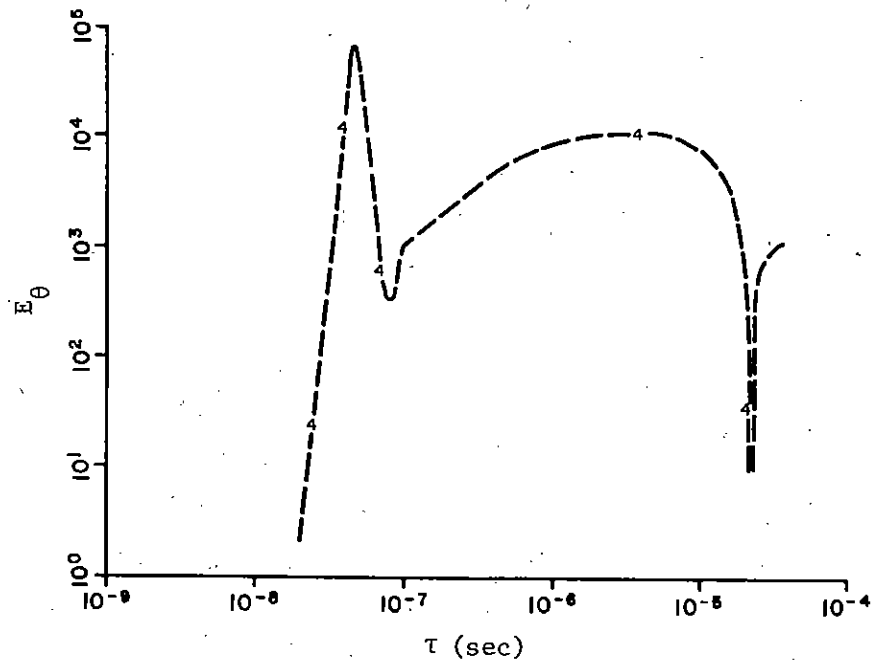

Fig. 18. Self-consistent theta electric field at 1000m, on the ground.

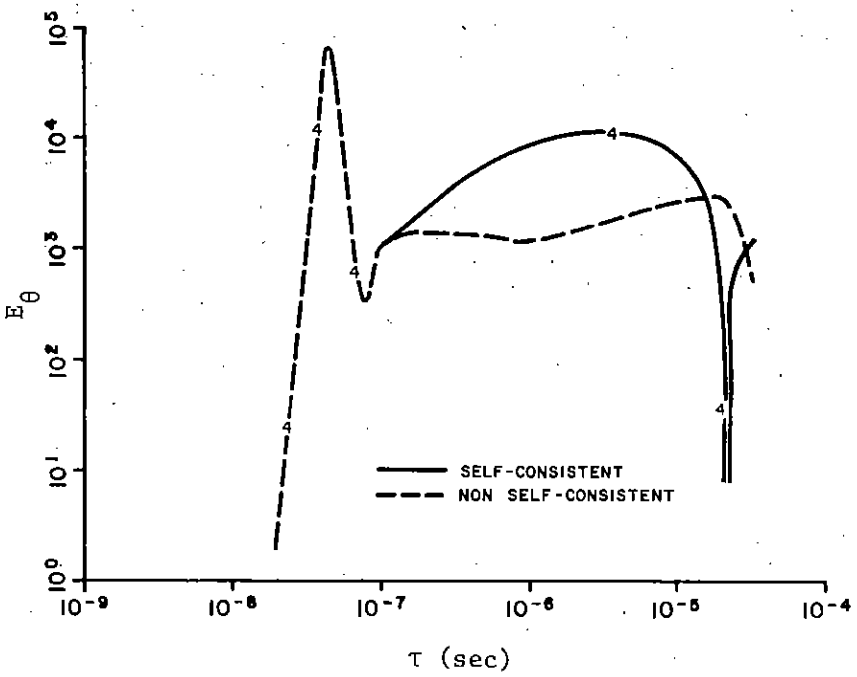

Fig. 19. Overlay, theta electric fields, 1000m.

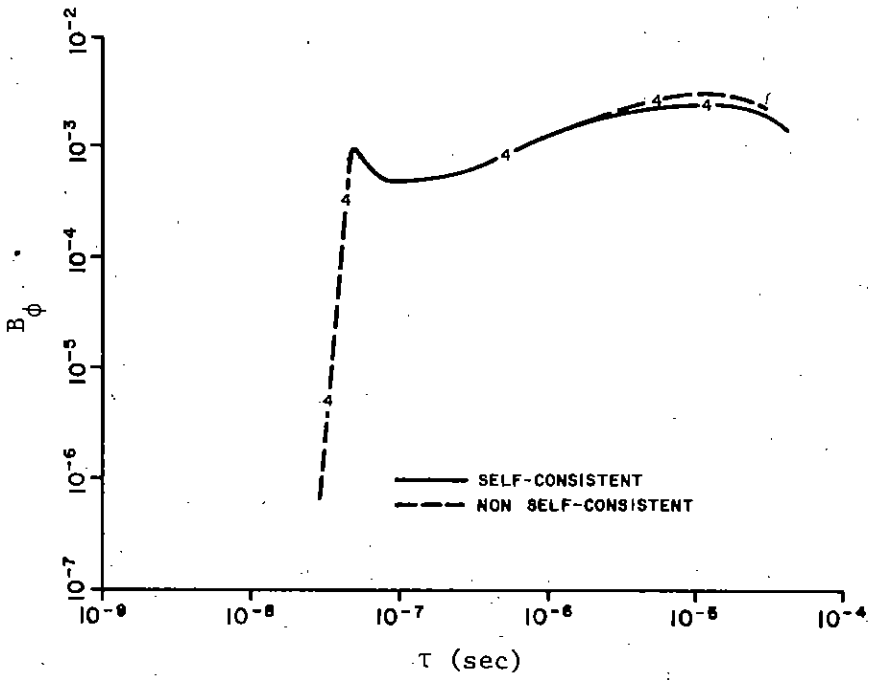

Fig. 20. Overlay, axial magnetic field, 1000m.

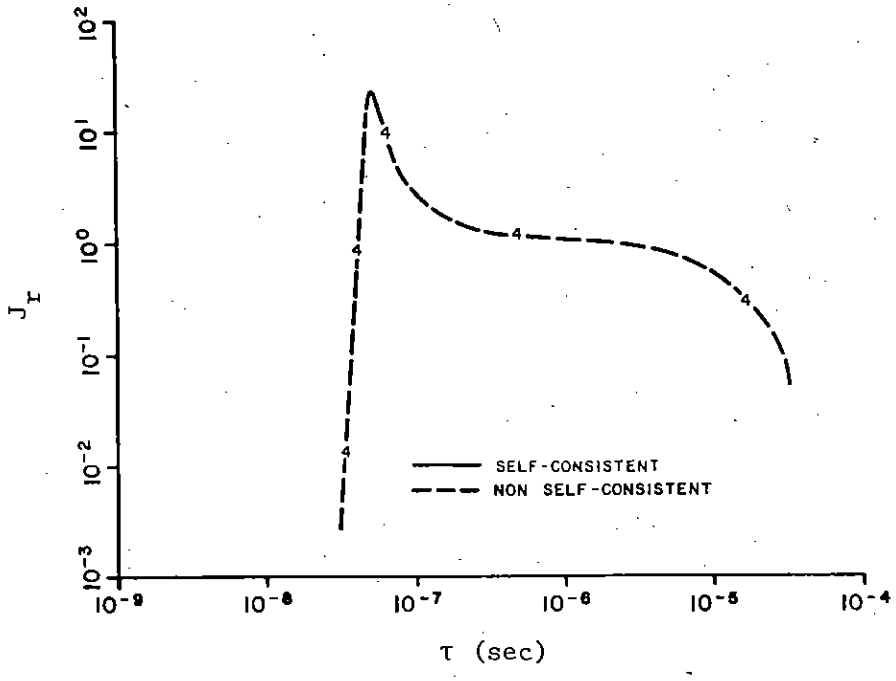

Fig. 21. Overlay, radial currents, 2000m.

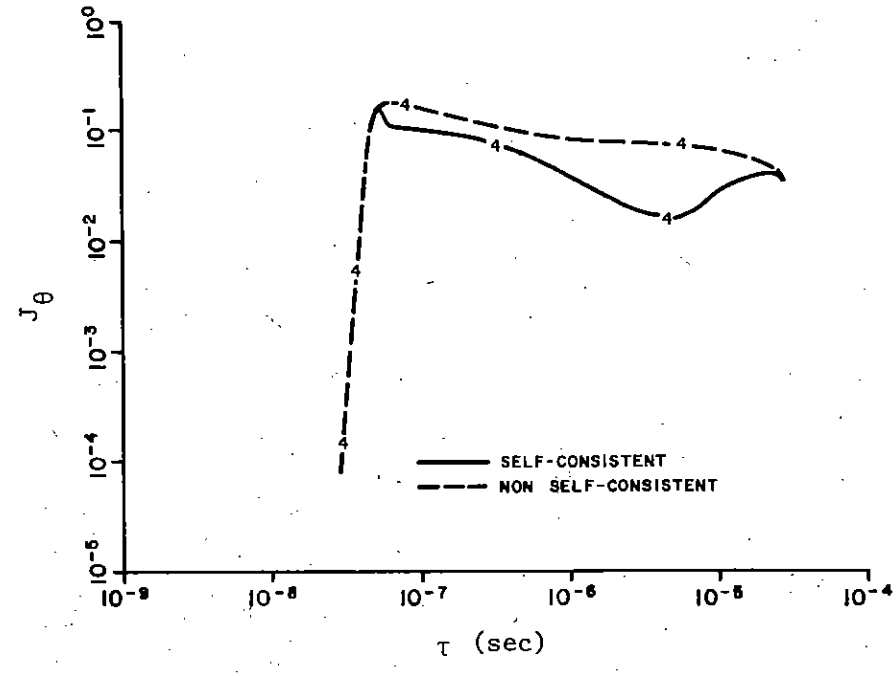

Fig. 22. Overlay, theta currents, 2000m.

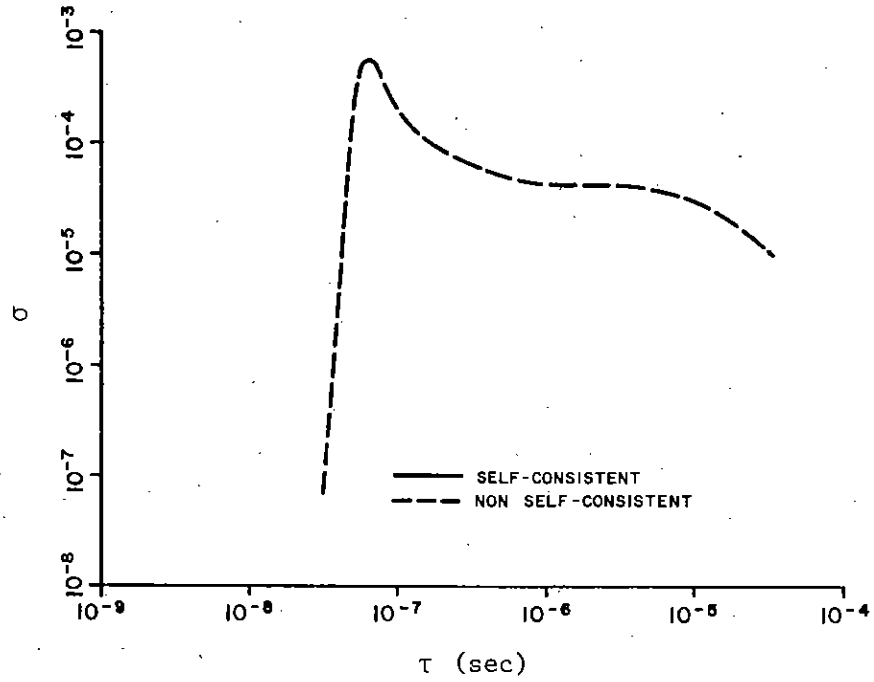

Fig. 23. Overlay, conductivity, 2000m.

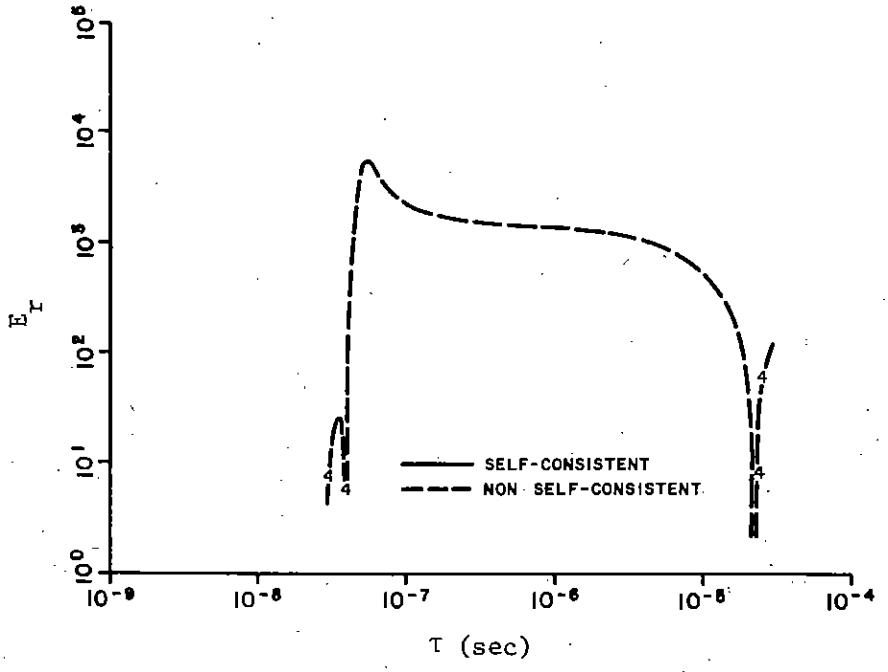

Fig. 24. Overlay, radial electric fields, 2000m.

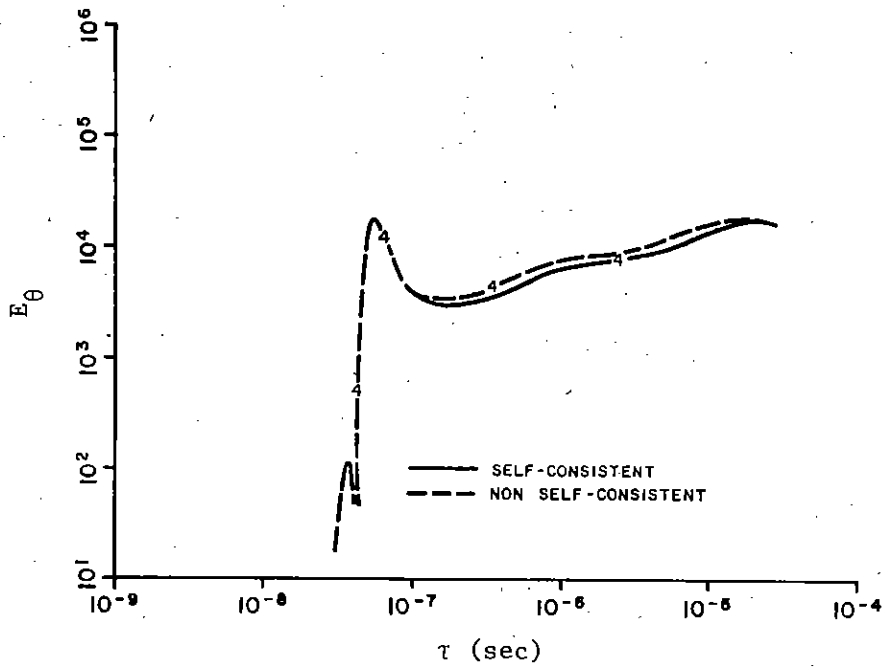

Fig. 25. Overlay, theta electric fields, 2000m.

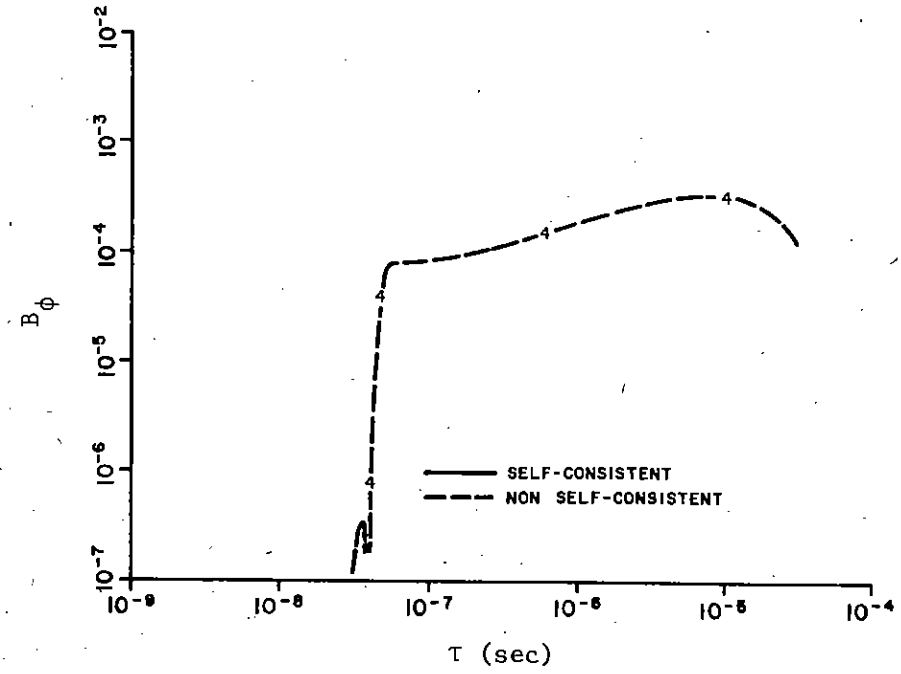

Fig. 26. Overlay, axial magnetic fields, 2000m.

SECTION V

RADIATION ENHANCED GROUND CONDUCTIVITY

In the past, SCX calculations have always assumed a uniform homogeneous ground with constant conductivity. However, in the real physical case, the deposition of radiation within the ground results in ionization which alters the conductivity from its ambient value. The time variation of the source and the nature of the deposition make the ground conductivity a function of both space and time. It is important to determine the effects of these possible variations on the EMP environments calculated with the SCX code.

To enhance calculational speed and efficiency, the coding in the SCX fields calculation has always implicitly assumed a constant ground conductivity. With the assumption of a variable conductivity, the differenced form of the radial equation in the ground becomes[3]

$$\left(\frac{1}{c_g^2} + \sigma_{ij}^{hk}\,\mu_g\,\frac{\delta t}{2}\right) E_{\rho_{ij}}^{hk} - \left(\frac{Z(\rho,z)}{2} - \frac{\delta t}{2\delta z_j}\right) B_{\phi_{ij}}^{k}$$

$$-\left(\frac{Z(\rho,z)}{2} + \frac{\delta t}{2\delta z_j}\right) B_{\phi_{ij-1}}^{k} = \left(\frac{1}{c_g^2} - \sigma_{ij}^{hk-1}\,\mu_g\,\frac{\delta t}{2}\right) E_{\rho_{ij}}^{hk-1}$$

$$-\left(\frac{Z(\rho,z)}{2} + \frac{\delta t}{2\delta z_j}\right) B_{\phi_{ij}}^{k-1} - \left(\frac{Z(\rho,z)}{2} - \frac{\delta t}{2\delta z_j}\right) B_{\phi_{ij-1}}^{k-1}$$

After the standard definition of constants, the following result is obtained

$$A1_j E_{\rho_{ij}}^{hk} - A21_j B_{\phi_{ij}}^{k} - A22_j B_{\phi_{ij-1}}^{k} = A3_j.$$

However, the following revised values of several constants must be used:

$$A1_j = \frac{1}{c_g^2} + \sigma_{ij}^{hk} \mu_g \frac{\delta t}{2}$$

$$A3_j = \left(\frac{1}{c_g^2} - \sigma_{ij}^{hk-1} \mu_g \frac{\delta t}{2} \right) E_{\rho_{ij}}^{hk-1}$$

$$-\left(\frac{Z(\rho,z)}{2} + \frac{\delta t}{2\delta z_j} \right) B_{\phi_{ij}}^{k-1} - \left(\frac{Z(\rho,z)}{2} - \frac{\delta t}{2\delta z_y} \right) B_{\phi_{ij-1}}^{k-1}$$

The other equation to be differenced which involves the conductivity is

$$R(\rho,z) \frac{\partial B_\phi}{\partial t} - \frac{1}{\rho} \frac{\partial}{\partial \rho}(\rho B_\phi) + \sigma \mu E_z \frac{1}{c_g^2} \frac{\partial E_z}{\partial \tau} = 0.$$

Assuming a variable conductivity, the following difference equation results

$$\left(R(\rho,z) - \frac{\rho_i}{\rho_i + \rho_{i-1}} \frac{\delta t}{\delta \rho}\right) B_{\phi_{ij}}^{k} + \left(\frac{1}{c_g^2} + \sigma_{ij}^{k} \mu_g \frac{\delta t}{2}\right) E_{z_{ij}}^{k}$$

$$= \left(\frac{1}{c_g^2} - \sigma_{ij}^{k-1} \mu_g \frac{\delta t}{2}\right) E_{z_{ij}}^{k-1} + \left(R(\rho,z) - \frac{\rho_i}{\rho_i + \rho_{i+1}} \frac{\delta t}{\delta \rho}\right) B_{\phi_{ij}}^{k-1}$$

$$- \left(\frac{\rho_{i-1}}{\rho_i + \rho_{i-1}} \frac{\delta t}{\delta \rho}\right) B_{\phi_{i-1j}}^{k} + \left(\frac{\rho_{i+1}}{\rho_i + \rho_{i-1}} \frac{\delta t}{\delta \rho}\right) B_{\phi_{i+1j}}^{k}$$

Definition of constants results in

$$A4_j B_{\phi_{ij}}^{k} + A5_j E_{z_{ij}}^{k} = A6_j \ ,$$

However, the following constants require new definition

$$A5_j = \frac{1}{c_g^2} + \sigma_{ij}^{k} \mu_g \frac{\delta t}{2} \quad (\neq A1_j \text{ for this case})$$

$$A6_j = \left(\frac{1}{c_g^2} - \sigma_{ij}^{k-1} \mu_g \frac{\delta t}{2}\right) E_{z_{ij}}^{k-1} + \left(R(\rho,z) - \frac{\rho_i}{\rho_i + \rho_{i+1}} \frac{\delta t}{\delta \rho}\right) B_{\phi_{ij}}^{k-1}$$

$$+ \left(\frac{\rho_{i+1}}{\rho_i + \rho_{i+1}} \frac{\delta t}{\delta \rho}\right) B_{\phi_{i+1j}}^{k-1} - \left(\frac{\rho_{i-1}}{\rho_i + \rho_{i-1}} \frac{\delta t}{\delta \rho}\right) B_{\phi_{i-1j}}^{k} \ .$$

When these changes are included in the field calculation subroutine of SCX, the effect of radiation enhanced ground conductivity may be examined.

Numerous models have been proposed to approximate the behavior of the ground conductivity with dose. To estimate the nature of the effect in SCX, it is convenient to use a simple model suggested by Graham and used by Jones[3]. In this approximation

$$\sigma_g(Q,z) = \sigma_g(\text{constant}) + \frac{1 \times 10^{-14}}{8.081 \times 10^{10}} \frac{34}{10^6} Qe^{20z}$$

where

Q is the ionization rate at the ground

$8.081 \times 10^{10} \frac{\text{mev}}{\text{m}^3}$ = 1 rad air

z is the depth in meters (a negative number), and

σ_g(constant) is the normal ground conductivity.

For a source on the ground, as is the case in SCX, the deposition beneath the surface is rather small for ranges greater than a few hundred meters. A typical value for the ground conductivity in SCX calculations is 0.01 mhos/meter. Figure 1 shows the radiation enhanced conductivity as a function of time 5 cm below the surface at a range of 250 meters in a typical SCX run. It can be seen that the values change by at most about 50% near the peak. Near the prompt peak, values of the transverse electric field on the

ground decrease by up to 30% for an observer at 250 meters. By 500 meters, the decrease is more like 5%. For the farther observers, the time histories compare within a line width. Thus, except for very close in observers there is little or no effect of enhanced conductivity on SCX results. This was the expected result for a ground burst due to the very small deposition in the ground. For a near surface case where the deposition can be orders of magnitude greater for down range observers, significant results would be expected.

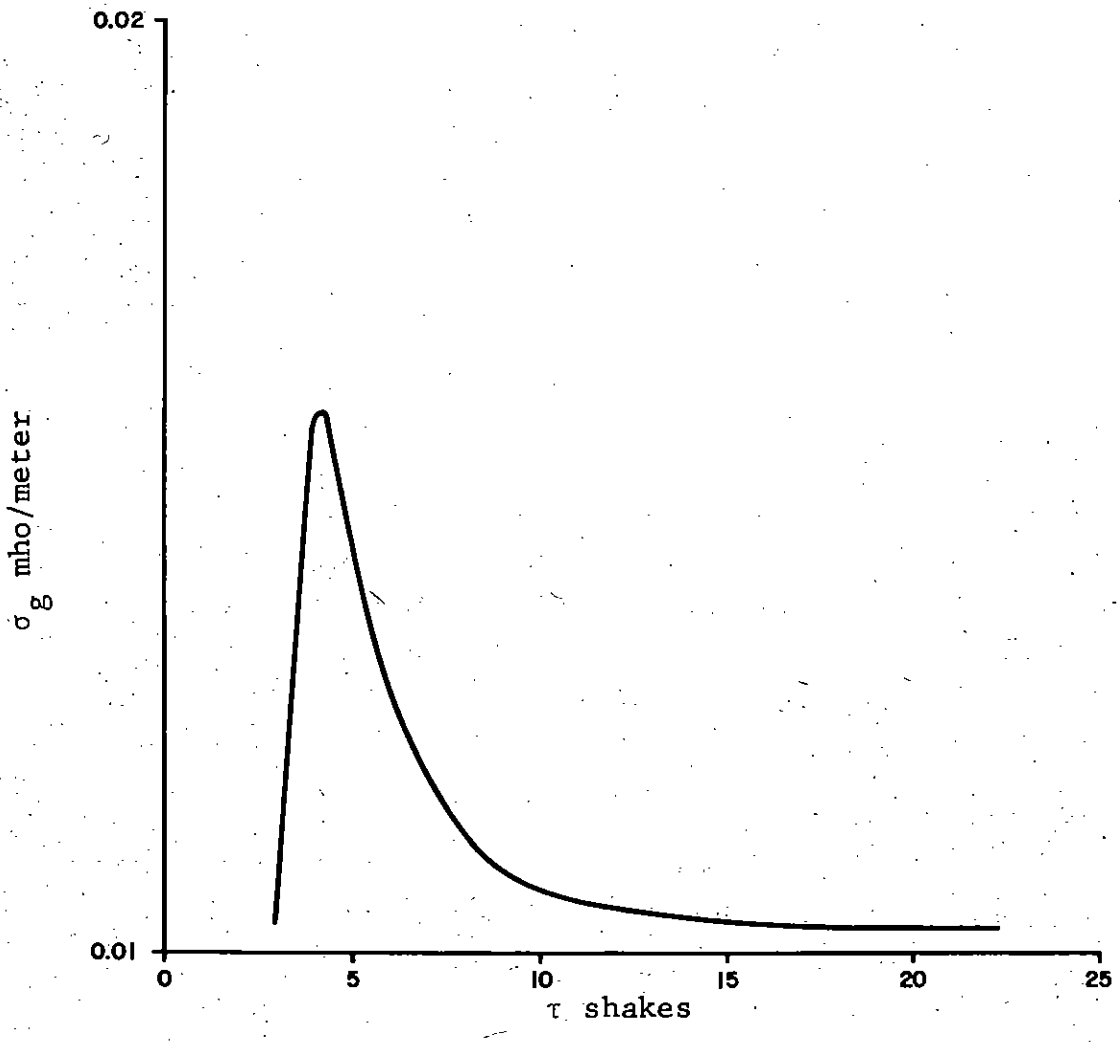

Figure 27. Radiation Enhanced Ground Conductivity vs. Time for Range of 250m and Depth of .05m.

REFERENCES

1. Dalich, S. J., "SCX: A Two-Dimensional Ground Burst EMP Code," SAI-73-501-AQ, June 1973.

2. Longley, H. J., "Compton Current in Presence of Fields for LEMP 1," EMP Theoretical Note 77, Vol. 2-4.

3. Jones, C. W., "EMP Comparisons of Photon Transport in the Vicinity of a Material Interface with Photon Transport in a Homogeneous Atmosphere," DC-TN-2153-2, 1972.